

# Three-dimensional Finite Element Buckling Analysis of Honeycomb Sandwich Composite Shells with Cutouts

J. Li, Z. H. Xiang, M. D. Xue<sup>1</sup>

**Abstract:** This paper investigates the buckling response of honeycomb sandwich composite shells with cutouts under axial compression. The Wilson's incompatible solid Finite Element (FE) is used around cutouts to obtain the detail stress distribution there. While to reduce the computational expense, a special multilayered relative degrees-of-freedom (DOF) shell FE is used to model the regions far from the cutouts. The efficiency and accuracy of this modeling scheme are illustrated by two benchmarks. Then parametric studies are carried out to reveal how the buckling response is influenced by the area, the shape and the orientation of cutouts.

**keyword:** Finite Element Method; Buckling analysis; Honeycomb Sandwich structure; Cutouts

## 1 Introduction

Honeycomb sandwich shells faced with fiber reinforced plastic sheets are finding various applications in aerospace structures due to their high strength-to-weight and stiffness-to-weight ratios and other attractive properties. However, these structures usually contain some cutouts or openings, in which complicated local buckling models are apt to occur during the launch period when the structures are subject to huge compressive loads.

Many approaches have been developed to analyze the buckling response of laminated composite structures with cutouts [Hilburger et al. (1999), Yazici et al. (2002), Jain and Kumar (2003), Tafreshi (2002)]. Most of them are based on equivalent-single-layer shell theories, such as the Mindlin theory and some high-order theories. Although these theories can satisfactorily predict the global buckling response of these structures, they could fail to deal with honeycomb sandwich shells, in which the

thicknesses and properties of sandwich core are quite different from those of face sheets. Layerwise theories [Reddy (1993)] and sandwich shallow shell theory [Livi and Terry (2000)] are designed for modeling the sandwich structures, but they still have some limitations for practical structural analysis, for example: (a) Shell elements always assume that the thickness of one element is uniform. However, the thickness of sandwich core or face sheets often varies in different parts continuously. If these shell elements are used, the discontinuous variation of the thickness would cause unrealistic stress concentration. (b) The transverse shear moduli of two composite laminate face sheets are much lower than their in-plane moduli. In addition, the moduli of sandwich core are very different from those of sandwich face sheets. Therefore, it is very difficult to obtain the accurate transverse shear stresses and interlayer stresses, which play a very important role in honeycomb sandwich shells. (c) The honeycomb sandwich structures often have geometric discontinuities, such as cutouts and local reinforcements, where significant stress concentration usually occurs. Under such circumstances, it is usually necessary to use some solid elements in these local areas. However, the connection of solid elements and shell elements is really troublesome and error prone. To overcome the above difficulties, modeling each part of honeycomb sandwich structures with three-dimensional solid elements seems a way out. However, owing to the high width-to-thickness ratio of each lamina and the big difference of the thickness among the sandwich core and the two face sheets, the FE mesh must be fine enough to ensure that these solid elements have a good shape ratio to avoid ill-conditioned stiffness matrices. This unavoidably leads to a very high computational expense for analyzing the whole structure. Especially for the buckling analysis, the large number of variables means an intolerable computing time and an inaccurate eigenvalue.

In this paper, a special three-dimensional FE scheme is adopted for modeling honeycomb sandwich structures.

---

<sup>1</sup> Corresponding author. Department of Engineering Mechanics, Tsinghua University, Beijing, 100084, P. R. China Tel.: +86-10-62772902; fax: +86-10-62781824; E-mail address: xuemd@mail.tsinghua.edu.cn

This scheme uses the Wilson incompatible solid element [Wilson et al. (1973)] to model the local stress concentration regions around cutouts and a laminated shell element with relative-DOF to model the smooth stress regions elsewhere. Two benchmarks are used to test the validity and accuracy of this scheme. Then numerical studies are performed to investigate the influence of the area, the shape and the orientation of cutouts to the buckling response of honeycomb sandwich cylindrical shells subjected to an axial compressive load.

## 2 Modeling Considerations

As mentioned above, if only ordinary solid elements are used, very fine FE mesh is needed to obtain the precise buckling responses of structure with cutouts. Computationally, this is too expensive to carry out the buckling analysis. However, if ordinary shell elements are adopted to reduce the DOF, we will suffer from the difficulty of modeling the honeycomb sandwich structures and connecting them with other elements. For this reason, special elements are needed.

### 2.1 16-node Wilson incompatible element

It is well known that with the help of the inner additional DOF, the precision of the Wilson incompatible element [Wilson et al. (1973)] can be greatly improved without increasing the mesh density. Therefore, it is beneficial to use such kind of element to model the part around cutouts. In this paper, a 16-node Wilson incompatible element (see Fig. 1) is adopted. The element displacement vector  $\mathbf{u}$  is expressed by nodal displacement vector  $\mathbf{u}^e$  and inner additional DOF vector  $\boldsymbol{\alpha}^e$  as follows:

$$\mathbf{u} = \sum_{i=1}^{16} N_i \mathbf{u}_i + \sum_{i=1}^5 G_i \boldsymbol{\alpha}_i \quad (1)$$

where

$$\boldsymbol{\alpha}_i^T = (\alpha_i, \beta_i, \gamma_i) (i = 1, 2, 3, 4, 5) \quad (2)$$

$N_i$  is the shape function, which is the same as that in ordinary 16-node solid element and  $G_i$  is the corresponding shape function of the inner additional DOF:

$$\begin{aligned} G_1 &= \xi(1 - \xi^2), & G_2 &= \eta(1 - \eta^2), \\ G_3 &= 1 - \xi^2, & G_4 &= \xi\eta(1 - \xi^2), \\ G_5 &= \xi\eta(1 - \eta^2) \end{aligned} \quad (3)$$

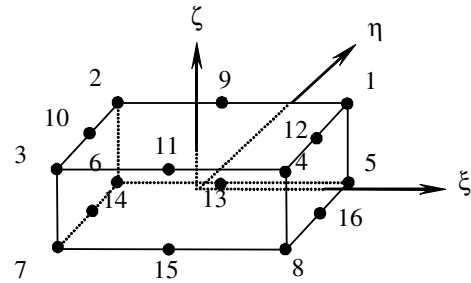


Figure 1 : The 16-node Wilson incompatible element.

### 2.2 Multilayered shell element with relative DOF

Introducing a kind of relative-DOF [Xiang et al.(2002)] to three-dimensional 16-node Wilson's incompatible element, a multilayered shell element is developed for the composite laminated shell, which is combined with  $n$  layers of 16-node relative-DOF shell elements (see Fig. 2). The transformations of nodal coordinates and displacement components of the  $k$ th layer are defined as follows:

$$\begin{cases} {}^k \mathbf{x}_i = {}^k \mathbf{x}_i - {}^k \mathbf{x}_{i+4} \\ {}^k \mathbf{x}_{i+4} = {}^k \mathbf{x}_{i+4} \end{cases} \quad \begin{cases} {}^k \bar{\mathbf{u}}_i = {}^k \mathbf{u}_i - {}^k \mathbf{u}_{i+4} \\ {}^k \bar{\mathbf{u}}_{i+4} = {}^k \mathbf{u}_{i+4} \end{cases} \quad (4)$$

$$i = 16(k-1) + j;$$

$$j = 1, 2, 3, 4, 9, 10, 11, 12$$

where  $i$  is the node number;  $\mathbf{x}_i^T = (x_i \ y_i \ z_i)$  is the nodal coordinate vector;  $\mathbf{u}_i^T = (u_{i1} \ u_{i2} \ u_{i3})$  is the nodal displacement vector;  $\bar{\mathbf{x}}_i^T = (\bar{x}_i \ \bar{y}_i \ \bar{z}_i)$  is the nodal relative coordinate vector and  $\bar{\mathbf{u}}_i^T = (\bar{u}_{i1} \ \bar{u}_{i2} \ \bar{u}_{i3})$  is the nodal relative displacement vector.

By means of standardized derivation [Li et al. (2005)], we obtain the shape functions  $\bar{N}_i$  of the 16-node relative DOF shell element as:

$$\begin{cases} \bar{N}_i = N_i \\ \bar{N}_{i+4} = N_i + N_{i+4} \end{cases} \quad (i = 1, 2, 3, 4, 9, 10, 11, 12) \quad (5)$$

Compared with the ordinary 16-node solid element, it is observed that in this 16-node relative-DOF shell element only the nodes on the upper face are relative, while the nodes on the lower face keep unchanged, which facilitates its connection with other solid elements. With the introduction of relative DOF instead of the customary shell rotation variables, this relative DOF shell element is very suitable for shell-type structure analysis. This is rigorously validated in reference [Worsak et al. (1981)].

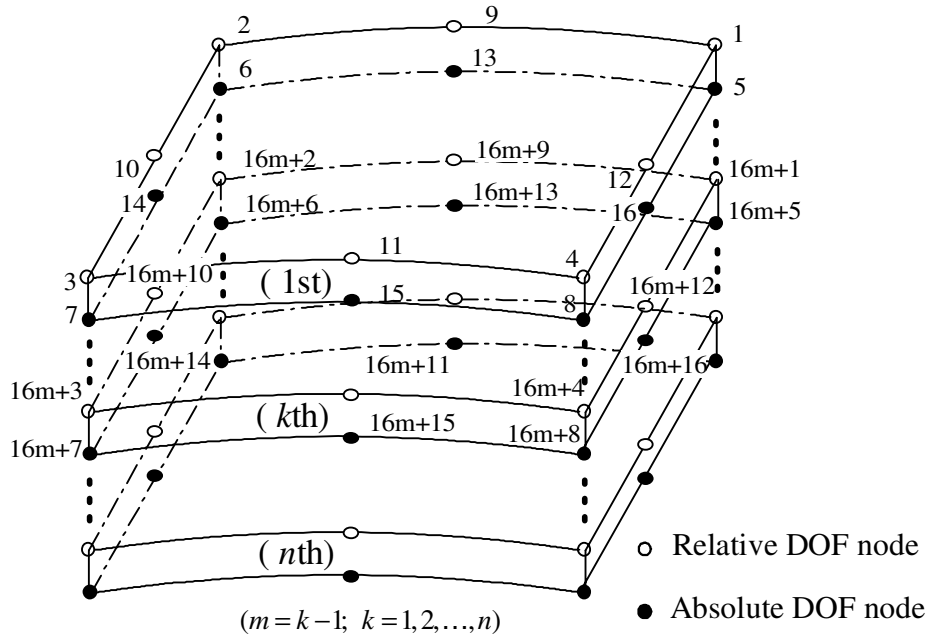


**Figure 2** :  $n$  layers of 16-node shell element with relative DOF.

Connecting the  $n$  16-node relative DOF shell elements layer by layer, the nodal displacement on lower surface of the  $(k-1)$ th layer and that on upper surface of the  $k$ th layer ( $k=2, 3, \dots, n$ ) should satisfy  $(n+1) \times 8 \times 3$  continuity conditions:

$$\begin{aligned} {}^{k-1}\bar{\mathbf{u}}_i &= {}^k\bar{\mathbf{u}}_j + {}^k\bar{\mathbf{u}}_{j+4} \\ (k=2, \dots, n; \quad m &= 16(k-2); \\ i &= m+5, m+6, m+7, m+8, m+13, \\ m+14, m+15, m+16; \\ j &= i+12) \end{aligned} \quad (6)$$

The above  $(n+1) \times 8 \times 3$  compatible conditions can be expressed as:

$$\mathbf{c}_{11}\bar{\mathbf{u}}_{(1)} + \mathbf{c}_{12}\bar{\mathbf{u}}_{(2)} = 0 \quad (7)$$

where the nodal relative displacement vectors  $\bar{\mathbf{u}}_i$  ( $i=1, 2, \dots, n \times 16$ ) are partitioned into two parts:  $\bar{\mathbf{u}}_{(1)}^T$  is an independent nodal relative displacement vector with  $(n+1) \times 8 \times 3$  components and  $\bar{\mathbf{u}}_{(2)}^T$  is a dependent nodal relative displacement vector with  $(n+1) \times 8 \times 3$  components. Details are:

$$\bar{\mathbf{u}}^T = (\bar{\mathbf{u}}_{(1)}^T, \bar{\mathbf{u}}_{(2)}^T) \quad (8)$$

$$\bar{\mathbf{u}}_{(1)}^T = ({}^1\bar{\mathbf{u}}_1^T, {}^1\bar{\mathbf{u}}_2^T, \dots, {}^1\bar{\mathbf{u}}_{16}^T; \dots; {}^k\bar{\mathbf{u}}_{m+5}^T \dots {}^k\bar{\mathbf{u}}_{m+8}^T, {}^k\bar{\mathbf{u}}_{m+13}^T \dots {}^k\bar{\mathbf{u}}_{m+16}^T; \dots) \quad (9a)$$

$$\bar{\mathbf{u}}_{(2)}^T = (\dots; {}^k\bar{\mathbf{u}}_{m+1}^T \dots {}^k\bar{\mathbf{u}}_{m+4}^T, {}^k\bar{\mathbf{u}}_{m+9}^T \dots {}^k\bar{\mathbf{u}}_{m+12}^T; \dots) \quad (9b)$$

$(m = 16(k-1); k = 2, \dots, n)$

These compatible conditions in Eq. (7) can be incorporated into the functional of the total potential energy  $W$  by the Lagrange multiplier vector  $\mathbf{\Lambda} = (\lambda_1, \lambda_2, \dots, \lambda_{24(n-1)})^T$  as follows:

$$\Pi = W + \mathbf{\Lambda}^T [\mathbf{c}_{11}\bar{\mathbf{u}}_{(1)} + \mathbf{c}_{12}\bar{\mathbf{u}}_{(2)}] \quad (10)$$

Using the principle of minimum total potential,  $\bar{\mathbf{u}}_{(1)}^T$ ,  $\bar{\mathbf{u}}_{(2)}^T$  and  $\mathbf{\Lambda}$  should satisfy the following equations:

$$\begin{bmatrix} \mathbf{K}_{11} & \mathbf{K}_{12} & \mathbf{c}_{11}^T \\ \mathbf{K}_{21} & \mathbf{K}_{22} & \mathbf{c}_{12}^T \\ \mathbf{c}_{11} & \mathbf{c}_{12} & 0 \end{bmatrix} \begin{Bmatrix} \bar{\mathbf{u}}_{(1)} \\ \bar{\mathbf{u}}_{(2)} \\ \mathbf{\Lambda} \end{Bmatrix} = \begin{Bmatrix} \mathbf{P}_{(1)} \\ \mathbf{P}_{(2)} \\ 0 \end{Bmatrix} \quad (11)$$

where  $\mathbf{K}_{ij}$  are the stiffness matrices of  $n$  layers of 16-node relative-DOF shell elements and  $\mathbf{P}_{(1)}$ ,  $\mathbf{P}_{(2)}$  are the nodal force vectors corresponding to  $\bar{\mathbf{u}}_{(1)}^T$  and  $\bar{\mathbf{u}}_{(2)}^T$ , respectively. From Eq. (11),  $\bar{\mathbf{u}}_{(1)}^T$  can be obtained as:

$$\begin{aligned} & [\mathbf{K}_{11} - \mathbf{K}_{12}\mathbf{K}_{22}^{-1}\mathbf{K}_{21} + \mathbf{A}^T(\mathbf{c}_{12}\mathbf{K}_{22}^{-1}\mathbf{c}_{12}^T)^{-1}\mathbf{A}] \bar{\mathbf{u}}_{(1)} \\ & = \mathbf{P}_{(1)} - (\mathbf{K}_{12} + \mathbf{A}^T\mathbf{c}_{12})\mathbf{K}_{22}^{-1}\mathbf{P}_{(2)} \end{aligned} \quad (12)$$

where

$$\mathbf{A} = \mathbf{c}_{11} - \mathbf{c}_{12}\mathbf{K}_{22}^{-1}\mathbf{K}_{21} \quad (13)$$

Then the independent nodal DOF vector  $\mathbf{u}^e$  of the resultant  $n$ -layered shell element (see Fig. 3) can be calculated by:

$$(\mathbf{u}^e)^T = (\bar{\mathbf{u}}_1, \bar{\mathbf{u}}_2, \dots, \bar{\mathbf{u}}_i, \dots, \bar{\mathbf{u}}_{8(n+1)}) = \bar{\mathbf{u}}_{(1)}^T \quad (14)$$

where

$$\begin{aligned} \bar{\mathbf{u}}_i &= {}^1\bar{\mathbf{u}}_i & (i \leq 16; k = 1) \\ \bar{\mathbf{u}}_i &= {}^k\bar{\mathbf{u}}_{i+8k-12} & (i \geq 16; k = 2, 4, 6, \dots; k \leq n) \\ \bar{\mathbf{u}}_i &= {}^k\bar{\mathbf{u}}_{i+8k+8} & (i \geq 16; k = 3, 5, 7, \dots; k \leq n) \end{aligned} \quad (15)$$

And the nodal displacement vector of resultant  $n$ -layered shell element  $\mathbf{u}_i$  can be calculated from relative DOF vector  $\bar{\mathbf{u}}_i$  as follows:

$$\begin{aligned} \mathbf{u}_i &= \bar{\mathbf{u}}_i + \bar{\mathbf{u}}_{i+4} & (i = 1, 2, 3, 4, 9, 10, 11, 12) \\ \mathbf{u}_i &= \bar{\mathbf{u}}_i & (i = 5, 6, 7, 8, 13 \leq i \leq 8(n+1)) \end{aligned} \quad (16)$$

### 2.3 Connection elements

Two types of connection element (shown in Fig. 4) are designed to connect the multilayered relative-DOF element with the ordinary solid element. In the Type I connection element, the connection interface is specified on the face of  $\eta = 1$ , where there are only three relative nodes. The corresponding transformation relation of shape functions is:

$$\begin{cases} \bar{N}_i = N_i & i = 1, 2, 3, 4, 7, 8, 9, 10, 11, 12, 13, 15, 16 \\ \bar{N}_{i+4} = N_i + N_{i+4} & i = 1, 2, 9 \end{cases} \quad (17)$$

While in the Type II connection element, the connection interfaces are specified on the faces of  $\eta = 1$  and  $\xi = -1$ , where there are five relative nodes. The corresponding transformation relation of shape functions is:

$$\begin{cases} \bar{N}_i = N_i & i = 1, 2, 3, 4, 8, 9, 10, 11, 12, 15, 16 \\ \bar{N}_{i+4} = N_i + N_{i+4} & i = 1, 2, 3, 9, 10 \end{cases} \quad (18)$$

Inner additional DOF can be added to the multilayered relative-DOF shell element and the two types of connection element by replacing the shape function  $\mathbf{N}$  in Eq. (1) with Eq. (5), Eq. (17) and Eq. (18), respectively.

The aforementioned modeling scheme can accurately predict the local response of complicated structures with reasonable computational expense. This ensures its promising application in the simulation of modern composite structures.

### 3 Verification of the Program

In order to verify this FE scheme, two benchmarks [Han and Simites (1991)] are examined. As Fig. 5 shows, they are buckling problems of a graphite epoxy-laminated cylindrical shell subjected to a uniform axial pressure and a uniform lateral pressure, respectively. In the lateral pressure case, the displacements  $u, v, w$  and the bending moments are all equal to zero at the middle layer of  $z = 0$  and  $z = L$ ; while in the axial pressure case, the boundary conditions are similar to that in the lateral pressure case, except that the displacement  $w$  is not constrained at the middle layer of  $z = L$ . The material properties<sup>2</sup> are

$$\begin{aligned} E_{11} &= 1.4966 \times 10^5 \text{ MPa}, \\ E_{22} &= E_{33} = 0.0993 \times 10^5 \text{ MPa}, \\ G_{12} &= G_{31} = 0.0448 \times 10^5 \text{ MPa}, \\ G_{23} &= 0.0388 \times 10^5 \text{ MPa}, \\ \nu_{21} &= \nu_{31} = \nu_{23} = 0.28 \end{aligned}$$

The FE meshes, which employ four-layered relative-DOF shell elements, are shown in Fig. 6. Owing to the symmetry of the problem, only the half-length model is considered for the lateral pressure case.

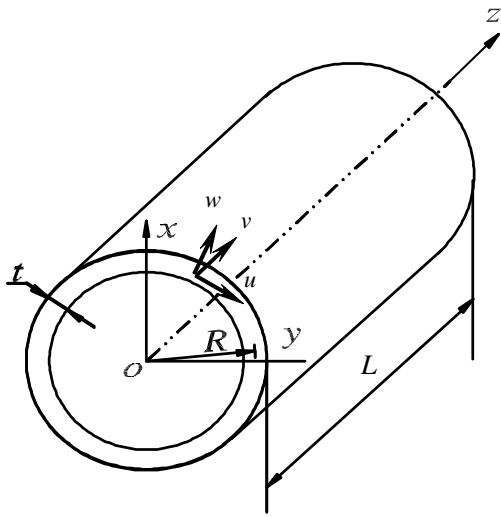
The numerical results are presented in Table 1, Table 2, Fig. 7 and Fig. 8. They are quite close to the theoretical solutions. The minor discrepancies are attributed to the assumption of the linear transverse shear deformation in Ref. [Han and Simites (1991)], which does not exist in the proposed FE models.

### 4 Buckling Analysis of Honeycomb Sandwich Cylindrical Shells with Cutouts

Once the confidence in the solution methodology is established, the buckling responses are studied for honeycomb sandwich cylindrical shells with different cutouts under a uniform axial compression.

<sup>2</sup>Only  $E_{11}, E_{22}, G_{12}$  and  $\nu_{21}$  are given in Ref. [Han and Simites (1991)]. To make the three-dimensional buckling analysis possible,  $E_{33}, G_{31}, G_{23}, \nu_{31}$  and  $\nu_{23}$  are added according to the transversely isotropic property of each ply.





$R = 19.05\text{cm}$   $L = 19.05\text{cm}$   $t = 0.3175\text{cm}$

**Figure 5 :** Graphite epoxy-laminated cylindrical shell.

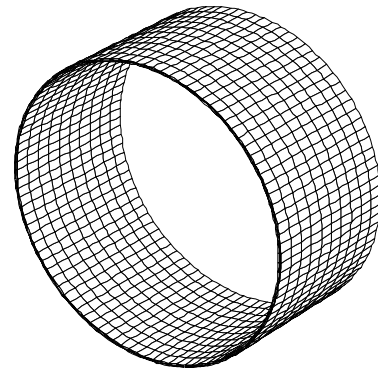
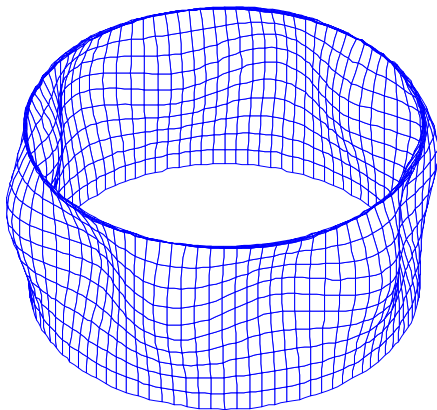
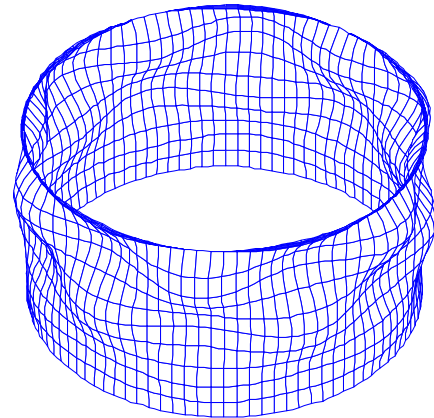


**Figure 6 :** The FE mesh of Graphite epoxy-laminated cylindrical shell.

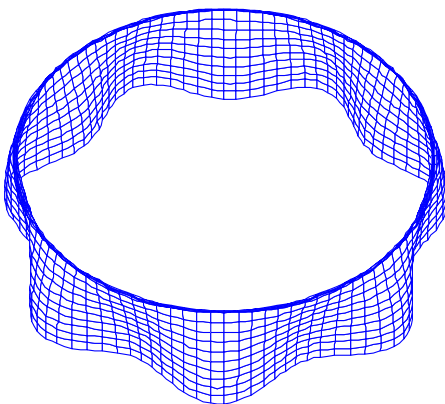


(a)  $[0_2/90_2]_s$

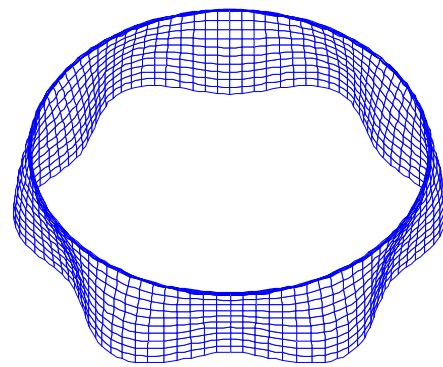


(b)  $[90_2/0_2]_s$

**Figure 7 :** The buckling modes of the laminated cylindrical shell under axial compression



(a)  $[0_2/90_2]_s$



(b)  $[90_2/0_2]_s$

**Figure 8 :** The buckling modes of the laminated cylindrical shell under lateral pressure

**Table 1** : The numerical results of axial compression case

Stack sequence	$[0_2/90_2]_s$		$[90_2/0_2]_s$	
	Critical load (kN/m)	Circumferential wavenumber	Critical load (kN/m)	Circumferential wavenumber
Present	768.2	6	711.1	6
Theoretical results	783.5	6	718.2	6

**Table 2** : The numerical results of lateral pressure case

Stack sequence	$[0_2/90_2]_s$		$[90_2/0_2]_s$	
	Critical load (kN/m <sup>2</sup> )	Circumferential wavenumber	Critical load (kN/m <sup>2</sup> )	Circumferential wavenumber
Present	962.2	7	2,361.7	6
Theoretical results	998.0	7	2,470.0	6

#### 4.1 Cylinder model and FE mesh

As Fig. 9 shows, the model analyzed in this study is a honeycomb sandwich cylindrical shell with Carbon Fiber Reinforced Plastic (CFRP) sheets. This shell could have a rectangular cutout or a circular cutout, where the shapes of cutouts are defined on developed surface of the shell. The dimensions of the shell are:  $R = 203.2$  mm,  $L = 406.4$  mm,  $t_c = 15.16$  mm,  $t_{top} = t_{bot} = 3.016$  mm, where  $R$  is the radius of the shell;  $L$  is the length of the shell;  $t_c$ ,  $t_{top}$  and  $t_{bot}$  are the thickness of the honeycomb core, upper and lower face sheet, respectively. The cutout is located at the middle of the shell. The cylinder is fully clamped on the bottom edge and clamped on the top edge except for axial motion. A uniform compressive load is applied on the top edge.

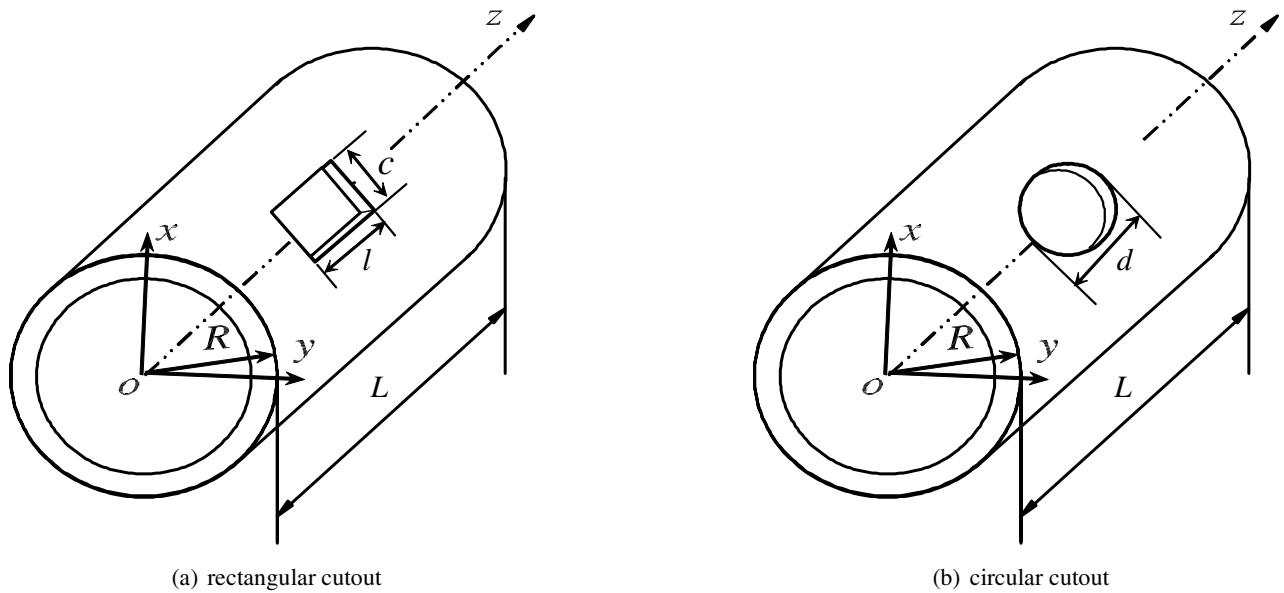
Twelve sandwich cylinder models, which have the same material properties (see Table 3) but have different cutouts, are analyzed. They are designed to study the effect of the area, the shape and the orientation of the cutout on the buckling load. Fig. 10 shows two typical FE meshes for the shell with a square developed cutout and a circular developed cutout, respectively. Each mesh has 27252 DOFs and is modeled by four kinds of elements: 1288 16-node Wilson elements in the first zone, 284 three-layered shell elements in the second zone, 40 Type I connection elements in the third zone and four Type II connection elements in the fourth zone. To obtain the first ten buckling loads, only about four minutes CPU time is needed on a personal computer (Pentium IV 3.0GHZ; 512M RAM).

#### 4.2 Results and discussion

Fig.11 and Fig.12 show the first four buckling modes of sandwich shells with a square developed cutout and a circular developed cutout, respectively. It should be noted that local buckling behaviors are observed around the cutout, which are caused by the local stress concentration in that region. These local buckling modes can hardly be found accurately by traditional methods. For example, using only the ordinary shell elements or a coarse solid element mesh one would probably lose such local modes; solving a fine solid element model is too time consuming and the corresponding buckling load could not be very accurate; although using shell elements to model the CFRP sheets and solid elements to model the honeycomb sandwich may reduce the computational expense, the connection of these two kinds of elements is still very difficult and error prone. It seems that the modeling strategy proposed here is an efficient way to solve this kind of problem.

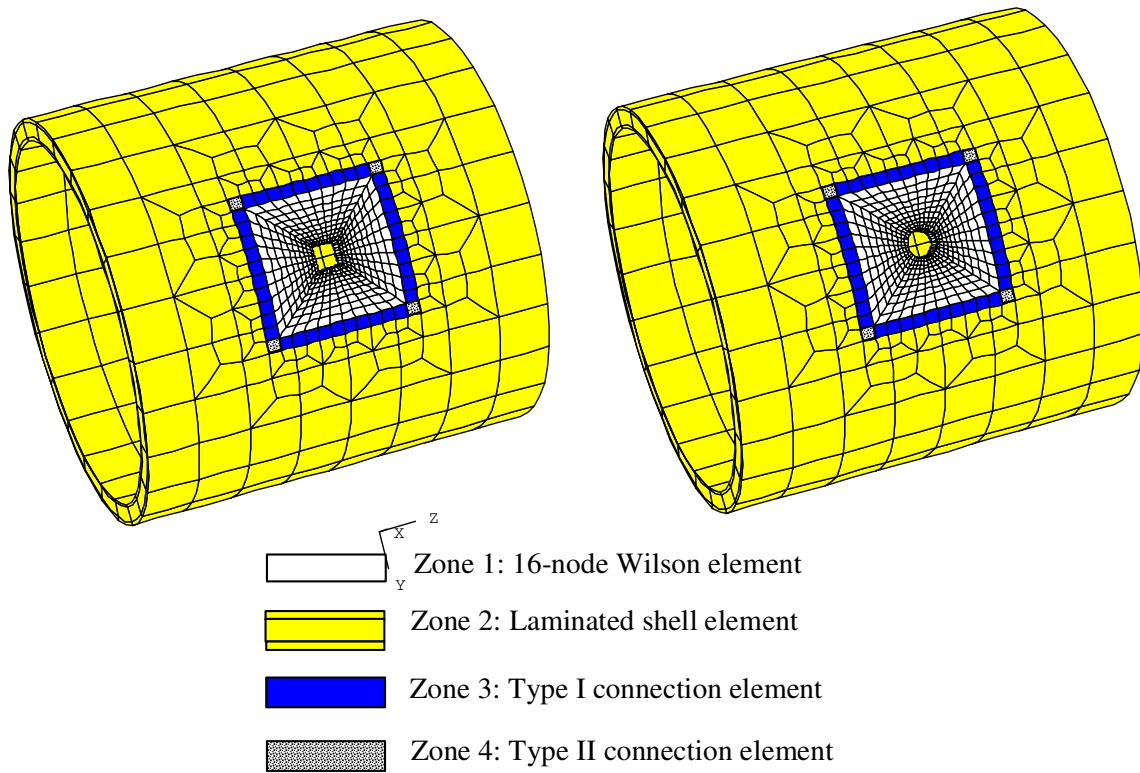
Fig.13 shows the variation of the normalized buckling load ( $P_{cr}/P_c$ ,  $P_{cr}$  and  $P_c$  are the buckling load with and without cutouts, respectively) versus the cutout size ( $\sqrt{A}/R$ ,  $A$  is the area of the cutout). It indicates that the buckling loads decrease greatly as the cutout area increases. Moreover, for models with equal developed areas of cutouts, the one with square cutout have larger decrease in the buckling load than the one with circular cutout. This is because the local stress concentration in square cutouts is sharper than that in circular cutouts.

Table 4 shows the buckling load of the honeycomb sand-



$$R = 203.2 \text{ mm } L = 406.4 \text{ mm}$$

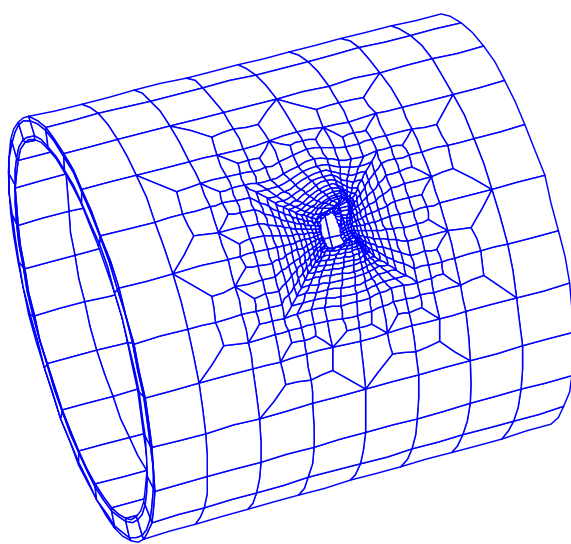
**Figure 9 :** The geometry of the honeycomb sandwich cylindrical shell with cutouts.



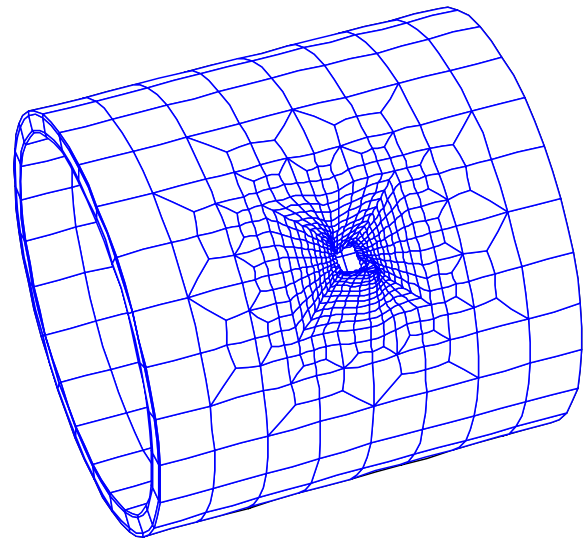
**Figure 10 :** The FE meshes of the honeycomb sandwich cylindrical shell with cutouts.

**Table 3** : The material properties of sandwich cylindrical shell

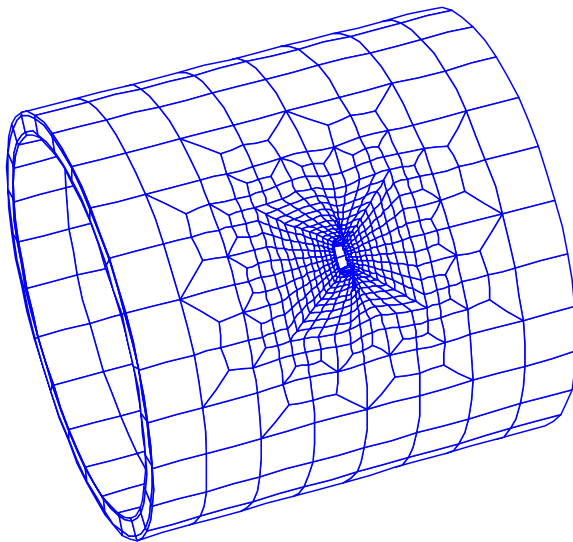
	$E_1$ (Gpa)	$E_2$ (Gpa)	$E_3$ (Gpa)	$G_{12}$ (Gpa)	$G_{23}$ (Gpa)	$G_{13}$ (GPa)	$\nu_{12}$	$\nu_{23}$	$\nu_{31}$
CFRP face sheets	23.98	23.98	3.72	9.37	3.57	3.57	0.28	0.034	0.3
Honeycomb core	$2.5 \times 10^{-4}$	$2.5 \times 10^{-4}$	0.12	$0.9 \times 10^{-4}$	0.129	0.129	0.35	0.3	$6.25 \times 10^{-4}$



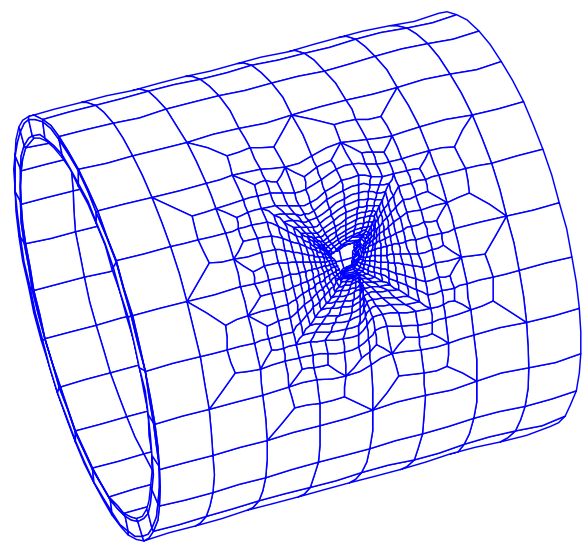
(a) the 1<sup>st</sup> buckling mode



(b) the 2<sup>nd</sup> buckling mode



(c) the 3<sup>rd</sup> buckling mode



(d) the 4<sup>th</sup> buckling mode

**Figure 11** : The first four buckling modes of the sandwich shell with a 25.4mm×25.4mm cutout subjected to an axial compressive load.

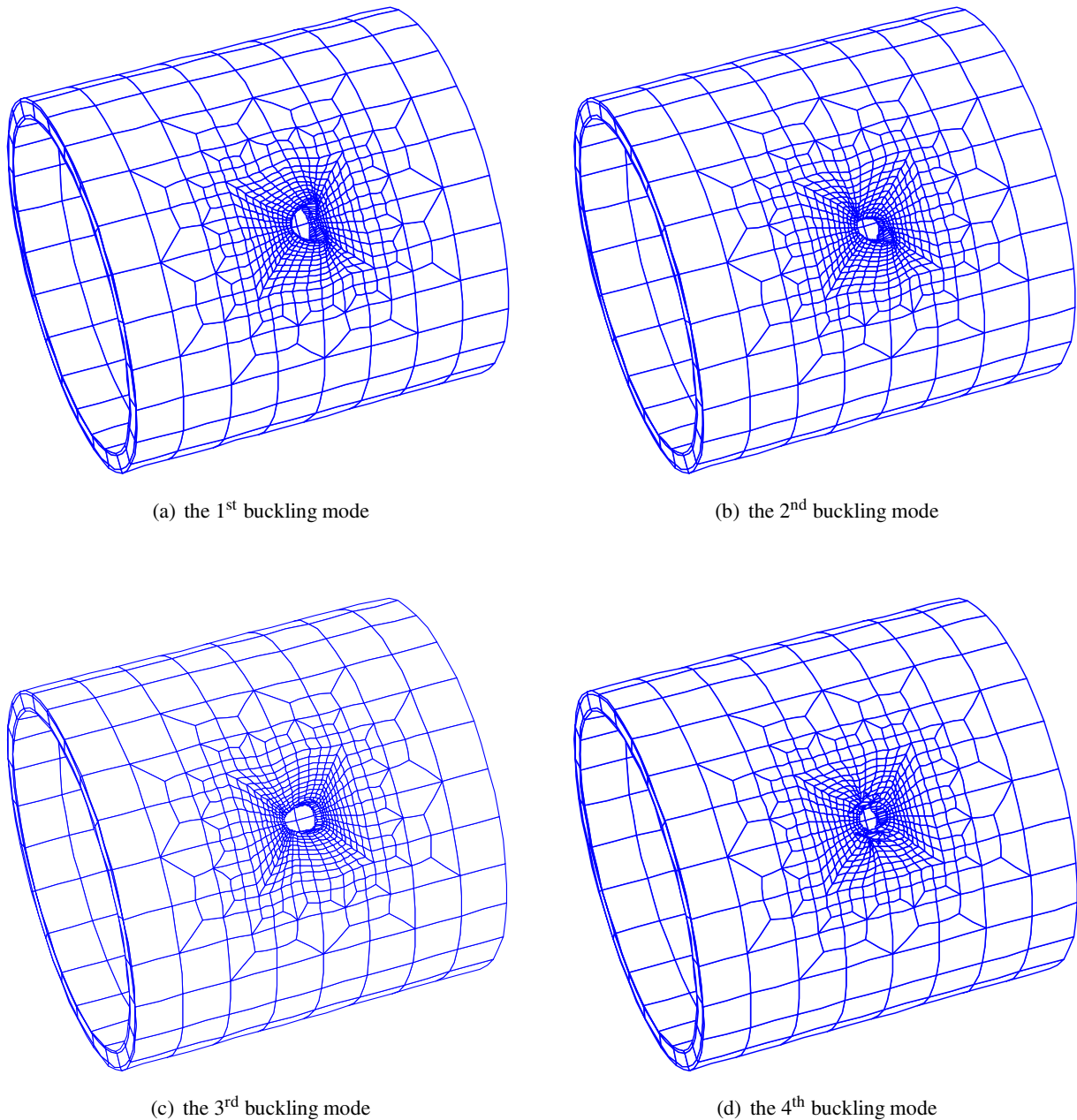


**Figure 12 :** The first four buckling modes of the sandwich shell with a 14.33 mm radius cutout subjected to an axial compressive load.

wich shells with six cutouts of the same developed area but of different shapes. The results indicate that the shell with circular cutout has the highest buckling load; the shell with square cutout ranks the second; the shell with the rectangular cutout with higher width (measurement in the circumferential direction) ranks the third and the shell with the rectangular cutout with higher length (measurement in the axial direction) has the lowest buckling load. It also noted that the buckling load of the shell with

50.8 mm × 12.7 mm cutout is 6.3% lower than that of the shell with the 12.7 mm × 50.8 mm cutout. This reveals the impact of the cutout orientation on the buckling load. It is concluded that among the rectangular cutouts with the same area, the one with higher width leads to a lower buckling load.

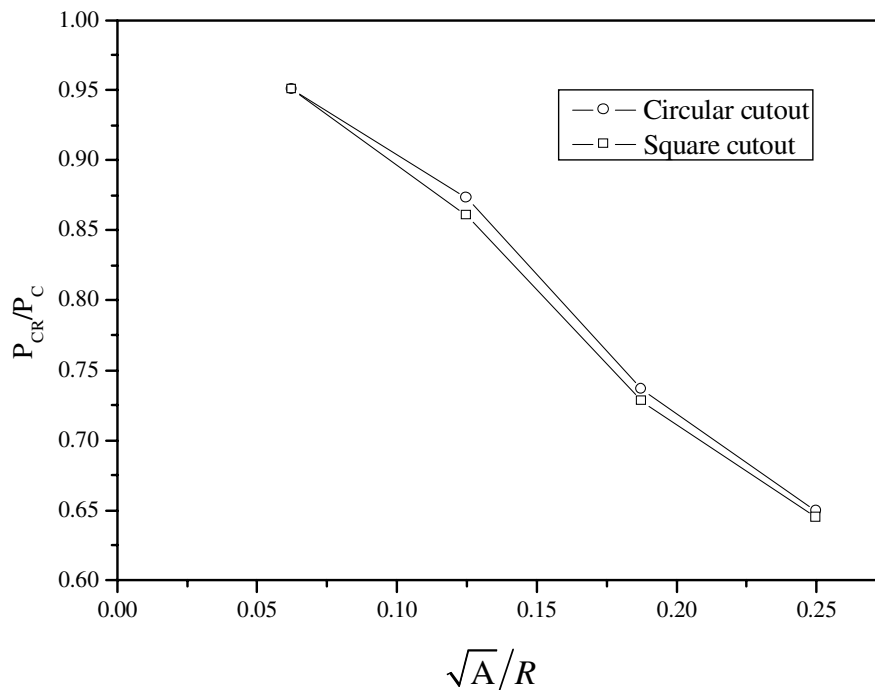


**Figure 13** : Variation of the normalized buckling loads of the sandwich shell with a cutout subjected to axial compression versus the change in cutout size ( $\sqrt{A}/R$ ).

**Table 4** : Buckling loads of the sandwich shell with a cutout for different shape cutouts

Cutout shape and size (mm)	Circle( $d$ )		Rectangle( $l \times c$ )			
		14.33	12.70× 50.80	16.93× 38.10	25.40× 25.40	38.10× 16.93
Buckling load (MPa)	170.54	164.84	166.89	168.09	164.06	154.96

### 5 Concluding remarks

In this paper, a special FE scheme is adopted to assess the buckling response of honeycomb sandwich cylindrical shells with cutouts under axial compression. This scheme utilizes the Wilson incompatible solid element to model the local stress concentration regions around cutouts and a laminated shell element with relative-DOF to model the smooth stress regions elsewhere. This modeling scheme greatly reduces the computational expense without losing the accuracy in regions of high local stress concentration. The numerical results show that the buckling load decreases as the cutout area increases. For the same cutout area, the shell with circular cutouts has higher buckling load than the shells with square cutouts and rectangular cutouts. Moreover, for the rectangular cutout of the same area, the cutout of higher width leads to lower buckling loads.

### References

**Chandra S. Yerramalli and Anthony M. Waas.**(2004): The Effect of Fiber Diameter on the Compressive Strength of Composites - A 3D Finite Element Based Study, *CMES: Computer Modeling in engineering & Sciences*, Vol. 6, No. 1, pp. 1-16 .

**Han, B.; Simites, G.J.** (1991): Analysis of anisotropic laminated cylindrical shells subjected to destabilizing loads. Part II. Numerical results. *Composite Structures*, vol. 17, pp. 183-205.

**Hilburger, M.W.; Waas, A.W.; Stames Jr. JH.** (1999): Response of composite shells with cutouts to internal pressure and compression loads. *AIAA J*; vol. 32, pp. 232-237.

**Jain, P.; Kumar, A.** (2003): Postbuckling response of square laminates with a central circular/elliptical cutout.

*Composite Structures*, vol. 65, pp. 179-185.

**Li, J.; Xiang, Z.H.; Xue, M.D.** (2005): Buckling analysis of rotationally periodic laminated composite shells by a new multilayered shell element. *Composite Structures*. (in press)

**Liviu, L.; Terry, H.** (2000): Recent developments in the modeling and behavior of advanced sandwich constructions: a survey. *Composite Structures*, vol. 48, pp. 1-17.

**Raghavan, P.; Ghosh, S.** (2004): Adaptive Multi-scale Computational Modeling of Composite Materials, CMES: *Computer Modeling in engineering & Sciences*, Vol. 5, No. 2, pp. 151-170.

**Reddy, J.N.** (1993): An evaluation of equivalent-single-layer and layerwise theories of composite laminates. *Composite Structures*, vol. 25, pp. 21-58.

**Tafreshi A.** (2002): Buckling and post-buckling analysis of composite cylindrical shells with cutouts subjected to internal pressure and axial compression loads. *International Journal of Pressure Vessels and Piping*, vol. 79, pp. 351-359.

**Wilson E.L.; Taylor, R.L.; Doherty, W.P. Ghaboussi, J.** (1973): Incompatible Displacement Models. In: Fenves, Steven J. (ed) *Numerical and Computer Methods in Structural Mechanics* [M]. New York: Academic Press Inc, pp. 43-59.

**Worsak, K.N.; Robert, L.T.; Thomas, J.R.** (1981): A large deformation formulation for shell analysis by the finite element method. *Computer & Structures*, vol. 13, pp. 19-27.

**Wu, C.P.; Chi, Y.W.** (2004): A Refined Asymptotic Theory for the Nonlinear Analysis of Laminated Cylindrical Shells, CMC: *Computers, Materials, & Continua*, Vol. 1, No. 4, pp. 337-352.

**Xiang, Z.H.; Xue, M.D.; Liu, Y.H.; Cen, Z.Z.** (2002): Finite element buckling analysis of rotationally periodic laminated composite shells. *International Journal for Numerical Methods in Engineering*, vol. 53, pp. 959-981.

**Yazici, M.; Ozcan, R.; Ulku, S.; Okur, I.** (2002): Buckling of composite plates with U-shaped cutouts. *Journal of Composite Materials*, vol. 37, pp. 2179-2195.